Erratum: "Numerical investigation of fast-wave propagation and radio-frequency sheath interaction with a shaped tokamak wall" [Phys. Plasmas 22, 072504 (2015)]

H. Kohno[1,a)], J. R. Myra[2], and D. A. D'Ippolito[2,*]

[1] *Department of Mechanical Information Science and Technology, Kyushu Institute of Technology, 680-4 Kawazu, Iizuka, Fukuoka 820-8502, Japan*

[2] *Lodestar Research Corporation, 2400 Central Avenue P-5, Boulder, CO 80301, USA*

[a)] Electronic mail: kohno@mse.kyutech.ac.jp

An error was discovered in the numerical code that was used for calculations in Sec. III of Ref. [1]. Specifically, although in this analysis the positive direction of the τ-axis along the sheath surface is defined as a counterclockwise direction, the unit vector $\mathbf{e}_\tau$ was erroneously turned in a clockwise direction (see Fig. 1(a) of Ref. [1]). Note that this error was not introduced into the numerical codes (rfSOL codes) for the previous calculations in slab geometry [2–4].

After correction, a singular behavior was observed in the calculated electric field near the "tangency points" (on the corners of the limiter protrusion) where the background magnetic field is tangent to the sheath surface. This is related to the fact that the absolute

[*] deceased, April 3, 2016

value of the wavenumber component tangential to the sheath surface, $|k_\tau|$, goes to infinity in the close vicinity of the tangency points as demonstrated in Ref. [4]. The reason for this may be understood heuristically as follows. The capacitive sheath boundary condition (BC) takes the form [5]

$$\mathbf{E}_{\mathrm{t}} = \nabla_{\mathrm{t}}\left(\frac{\Delta_{\mathrm{sh}}}{\varepsilon_{\mathrm{sh}}} D_{\mathrm{n}}\right) \approx \nabla_{\mathrm{t}}\left(\Delta_{\mathrm{sh}} b_{\mathrm{n}} \varepsilon_{\|} E_{\|}\right),$$

where Δ_{sh} is the nonlinear time-averaged sheath width, D_{n} ($= \varepsilon_0 \mathbf{s}\cdot\boldsymbol{\varepsilon}\cdot\mathbf{E}$) is the component of the electric displacement normal to the sheath (and $\mathbf{s}$ is the unit normal vector pointing into the plasma), b_{n} is defined by $b_{\mathrm{n}} = \mathbf{b}\cdot\mathbf{s} = \mathbf{B}_0\cdot\mathbf{s}/|\mathbf{B}_0|$ where $\mathbf{B}_0$ is the background magnetic field, and the final approximate form assumes that the contribution $\varepsilon_{\|}$ is dominant. Near a tangency point, b_{n} goes to zero and we would expect to recover the usual conducting-wall BC, $\mathbf{E}_{\mathrm{t}} \to \mathbf{0}$, because when the magnetic field is parallel to the surface, the electron-poor sheath on which the capacitive sheath BC is based does not exist. However, another solution is possible and can dominate the results, namely, $\nabla_{\mathrm{t}} \to \infty$ as $b_{\mathrm{n}} \to 0$.

To avoid numerical instability caused by this singularity especially in the nonlinear regime where the sheath voltage is high, the capacitive sheath BC, which is shown in Eq. (2) in Ref. [1], is slightly modified as follows:

$$\mathbf{E}_{\mathrm{t}} - a_{\mathrm{s}}^2 \frac{\partial^2 E_\tau}{\partial \tau^2}\mathbf{e}_\tau = \nabla_{\mathrm{t}}\left(\frac{\Delta_{\mathrm{sh}}}{\varepsilon_{\mathrm{sh}}} D_{\mathrm{n}}\right), \tag{2}$$

where a_{s} is the smoothing coefficient. The second term on the left-hand side of Eq. (2) is an additional term, not present in the sheath BC derived in Ref. [5] that is added for both numerical and physical reasons; it effectively filters out extremely fast variations along the surface from the solution for E_τ. Physically, we expect other terms to enter the dielectric response in D_{n} when the scale length of the electric field is so small that it becomes comparable to other characteristic scales that are not in the fluid description. For example, electron kinetic effects will enter $\varepsilon_{\|}$ when the parallel scale length is of order v_{te}/ω ~ 3×10^{-3} m. (Note that near the tangency point, the τ direction is almost parallel to the magnetic field.) Also, nonlinear effects enter the electron dielectric response when the parallel scale length is of the order of the characteristic electron jitter distance $\xi_{\|}$ ~ $eE_{\|}/m_{\mathrm{e}}\omega^2$ ~ 3×10^{-3} m. Finally, as noted previously, the structure of the sheath itself requires generalization near the tangency point. All of these issues are beyond the scope of this paper.

The calculations in Ref. [1] have been redone using the modified rfSOL code. Here, the parameters described in Sec. III of Ref. [1] remain the same, except that the number of the nine-node elements in the calculation domain is increased from 157696 to 332800, the smoothing coefficient a_{s} is fixed at 0.02 m, and the maximum antenna surface current density $K_{\max}$ is reduced from 3 kA/m to 1.5 kA/m for the base case; an exception is the analysis for the investigation of dependence on plasma density (Sec. III D) where the maximum antenna surface current and the protrusion height h_{p} are fixed at 2 kA/m and 0.02

m, respectively, with the other base case parameters kept unchanged. Figures 3–9 show the obtained numerical results, each of which replaces the corresponding figures in Ref. [1]. The electric fields shown here correspond to the ones on the plane of $z = 0$ at $t = 2\pi l/\omega$, where l in an integer. It can be seen that most of the figures are qualitatively similar to those in the original paper although the plots quantitatively change by a factor of two or more. Therefore, it is important to note that our previous qualitative and conceptual conclusions still hold. The main change is that the RF sheaths generated by the FW to SW conversion process for a given value of FW electric field are now somewhat larger. In particular, the strongly nonlinear response for $V_{\mathrm{sh}} > 100$ V around 160 degrees for the base case could be attributed to the sheath-plasma resonance at the tangency point where $|k_\tau|$ goes to infinity.

In addition to our previous work in slab geometry [4], this research also highlights the importance of near-tangency interactions. This is an important discovery since present models indicate that large sheath voltages develop there as a result. Our work therefore motivates further development of wave and sheath models for grazing incidence magnetic field lines and tangency points. Special attention should be paid to dissipation mechanisms that might provide a rigorous closure of the model for short-scale variations along the sheath surface.

As a final remark, because of the addition of the smoothing term Eqs. (A8) and (A9) in Ref. [1] are replaced with the following expressions:

$$G_{\tau i} \equiv \left(\left[N_i^{\mathrm{S}} N_j^{\mathrm{S}}\right] + a_{\mathrm{s}}^2 \left[\breve{N}_i^{\mathrm{S}} \breve{N}_j^{\mathrm{S}}\right]\right) \hat{E}_{\tau j}^{\mathrm{S}} - \left[N_i^{\mathrm{S}} \breve{N}_j^{\mathrm{S}} \breve{N}_k^{\mathrm{S}} \breve{N}_l^{\mathrm{S}}\right] \mathbf{s}_k \cdot \boldsymbol{\chi}_l \cdot \hat{\mathbf{E}}_j^{\mathrm{S}} = 0, \tag{A8}$$

where

$$\begin{aligned}
&\left[N_i^{\mathrm{S}} N_j^{\mathrm{S}}\right] \equiv \int_{\Gamma^{\mathrm{S}}} N_i^{\mathrm{S}} N_j^{\mathrm{S}} \mathrm{d}\Gamma^{\mathrm{S}}, \\
&\left[\breve{N}_i^{\mathrm{S}} \breve{N}_j^{\mathrm{S}}\right] \equiv \int_{\Gamma^{\mathrm{S}}} \frac{\mathrm{d}N_i^{\mathrm{S}}}{\mathrm{d}\tau} \frac{\mathrm{d}N_j^{\mathrm{S}}}{\mathrm{d}\tau} \mathrm{d}\Gamma^{\mathrm{S}}, \\
&\left[N_i^{\mathrm{S}} \breve{N}_j^{\mathrm{S}} \breve{N}_k^{\mathrm{S}} \breve{N}_l^{\mathrm{S}}\right] \equiv \int_{\Gamma^{\mathrm{S}}} N_i^{\mathrm{S}} \frac{\mathrm{d}}{\mathrm{d}\tau} \left(N_j^{\mathrm{S}} N_k^{\mathrm{S}} N_l^{\mathrm{S}}\right) \mathrm{d}\Gamma^{\mathrm{S}}.
\end{aligned} \tag{A9}$$

Figure Captions

FIG. 3. (Color online) Filled contour plots of $\mathrm{Re}(E_{\perp y})$ (a), $\mathrm{Re}(E_{\|})$ (b) and its expanded view near the edge of the limiter protrusion (c) for the base case. Note that the FW-to-SW conversion occurs where the contact angle changes rapidly.

FIG. 4. (Color online) RF sheath voltage V_{sh} vs. the poloidal angle θ for four different heights of the limiter protrusion: (a) wide-range profiles; and (b) localized profiles at the edge of the protrusion. The peak sheath voltage of about 195 V occurs for the case where $h_{\mathrm{p}} = 0.03\ \mathrm{m}$ (the base case) and decreases with decrease in h_{p}.

FIG. 5. Plots of the real part of $E_{\perp y}$ and $|b_n|$ as functions of the poloidal angle θ for $h_{\mathrm{p}} = 0\ \mathrm{m}$ (a) and $h_{\mathrm{p}} = 0.03\ \mathrm{m}$ (the base case) (b).

FIG. 6. (Color online) RF sheath voltage V_{sh} vs. the poloidal angle θ for four different values of k_z at the edge of the limiter. The peak sheath voltage of about 195 V occurs for the case where $k_z = 2.7\ \mathrm{m}^{-1}$ (the base case) and decreases rapidly with increase in k_z.

FIG. 7. (Color online) Filled contour plot of $\mathrm{Re}(E_{\perp y})$ for the case of $k_z = 10.8\,\mathrm{m}^{-1}$. Here, the blue line denotes the FW cutoff. Notice that the FW evanescent electric fields do not reach the limiter protrusion.

FIG. 8. (Color online) (a) RF sheath voltage V_{sh} vs. the poloidal angle θ for four different values of the edge plasma density $n_{\mathrm{e}}|_{\Psi_{\mathrm{p}}=\infty}$; and (b) filled contour plot of $\mathrm{Re}(E_{\parallel})$ for the case of $n_{\mathrm{e}}|_{\Psi_{\mathrm{p}}=\infty} = 4\times10^{17}\ \mathrm{m}^{-3}$. The peak sheath voltage of about 210 V occurs for the case where $n_{\mathrm{e}}|_{\Psi_{\mathrm{p}}=\infty} = 4\times10^{17}\ \mathrm{m}^{-3}$ and decreases with increase in $n_{\mathrm{e}}|_{\Psi_{\mathrm{p}}=\infty}$. Note that the maximum antenna surface current density K_{max} and the protrusion height h_{p} are fixed at 2 kA/m and 0.02 m, respectively.

FIG. 9. Comparison of the RF sheath voltage V_{sh} (a) and the real part of $E_{\perp y}$ (b) as functions of the poloidal angle θ along the sheath surface between the cases of $\nu_{\mathrm{i0}} = 0.2\omega$ (the base case) and $\nu_{\mathrm{i0}} = 0.4\omega$.

References

[1] H. Kohno, J. R. Myra, and D. A. D'Ippolito, Phys. Plasmas **22**, 072504 (2015).

[2] H. Kohno, J. R. Myra, and D. A. D'Ippolito, Comput. Phys. Commun. **183**, 2116 (2012).

[3] H. Kohno, J. R. Myra, and D. A. D'Ippolito, Phys. Plasmas **19**, 012508 (2012).

[4] H. Kohno, J. R. Myra, and D. A. D'Ippolito, Phys. Plasmas **20**, 082514 (2013).

[5] D. A. D'Ippolito and J. R. Myra, Phys. Plasmas **13**, 102508 (2006).

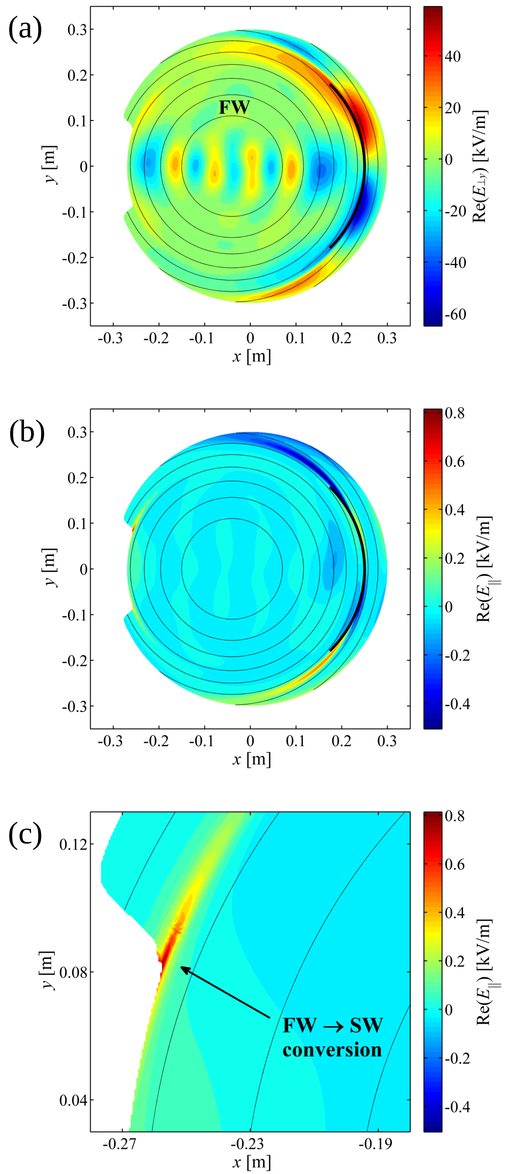
(a)
FW
y [m]
x [m]
Re($E_{\perp y}$) [kV/m]
(b)
y [m]
x [m]
Re($E_{\|}$) [kV/m]
(c)
FW → SW
conversion
y [m]
x [m]
Re($E_{\|}$) [kV/m]

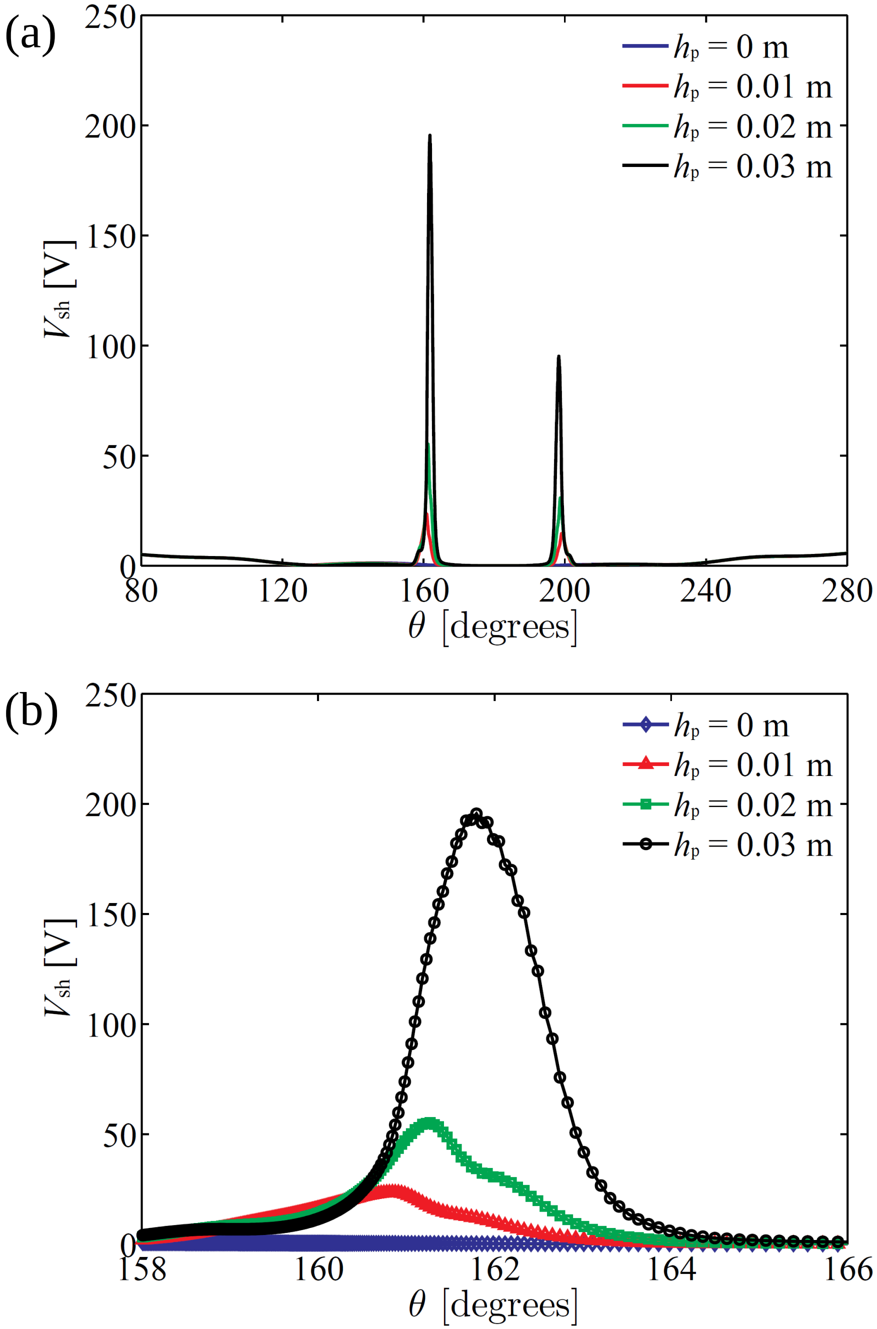

(a)
(b)
h_p = 0 m
h_p = 0.01 m
h_p = 0.02 m
h_p = 0.03 m
V_{sh} [V]
θ [degrees]
0
50
100
150
200
250
80
120
160
200
240
280
158
160
162
164
166

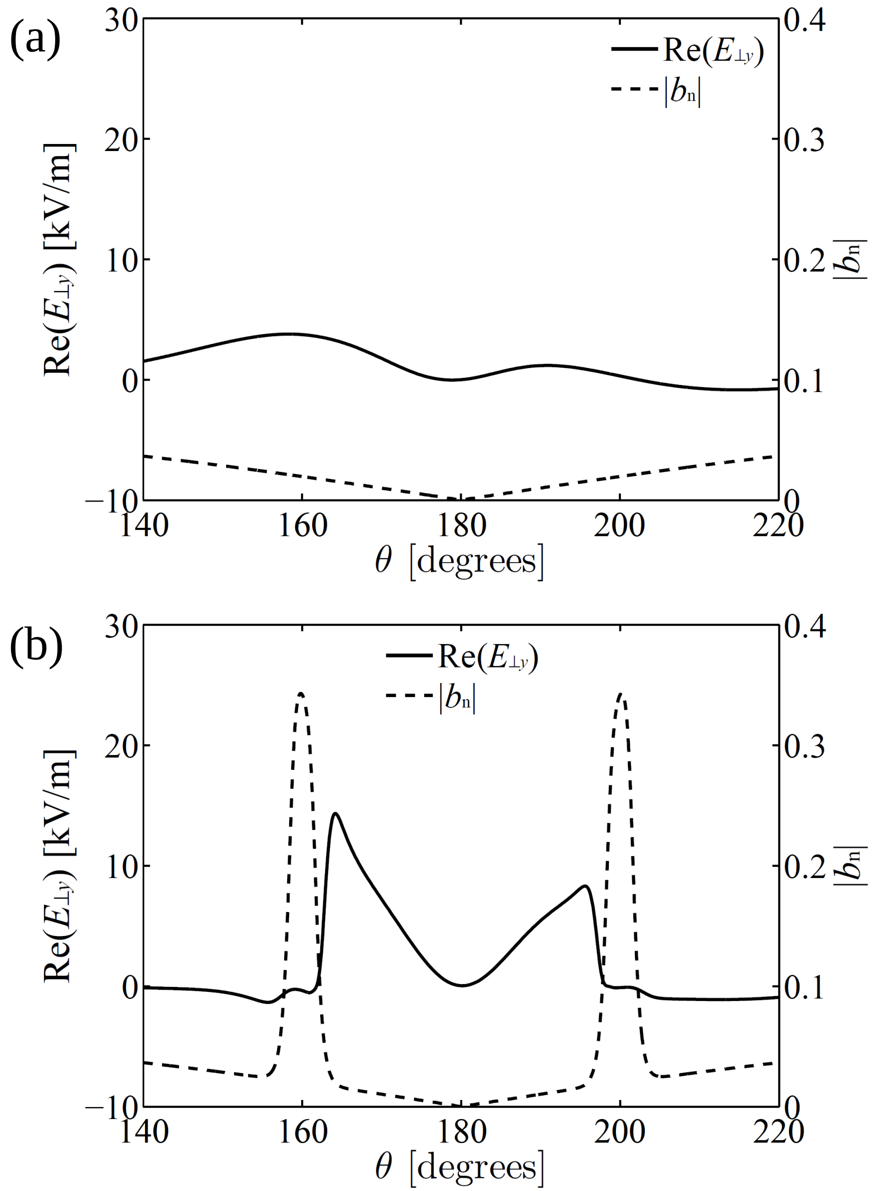
(a)
Re($E_{\perp y}$)
$|b_n|$
Re($E_{\perp y}$) [kV/m]
$|b_n|$
30
20
10
0
−10
0.4
0.3
0.2
0.1
0
140
160
180
200
220
θ [degrees]
(b)
Re($E_{\perp y}$)
$|b_n|$
Re($E_{\perp y}$) [kV/m]
$|b_n|$
30
20
10
0
−10
0.4
0.3
0.2
0.1
0
140
160
180
200
220
θ [degrees]

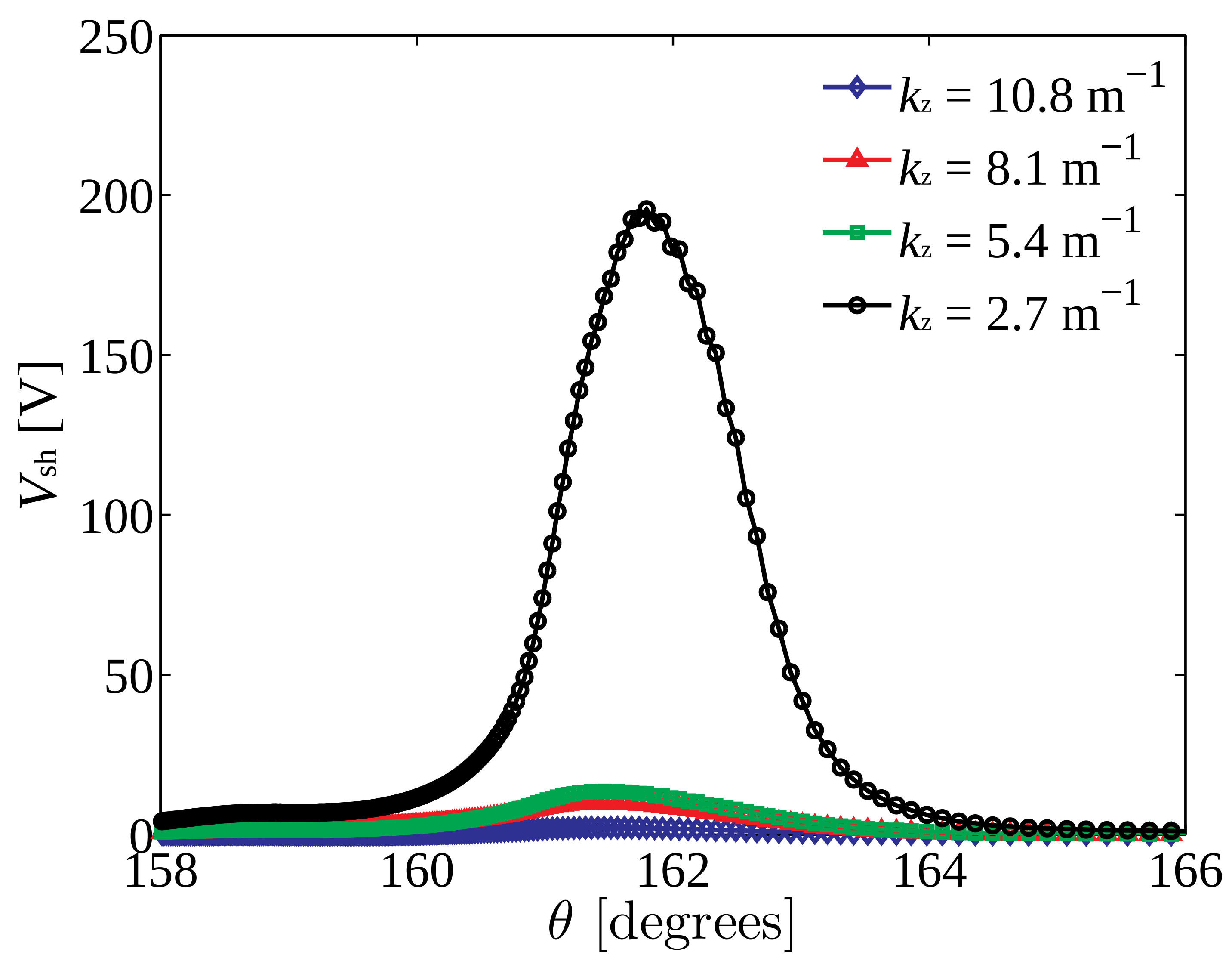

250
200
150
100
50
0
158
160
162
164
166
V_{sh} [V]
θ [degrees]
$k_z = 10.8\ m^{-1}$
$k_z = 8.1\ m^{-1}$
$k_z = 5.4\ m^{-1}$
$k_z = 2.7\ m^{-1}$

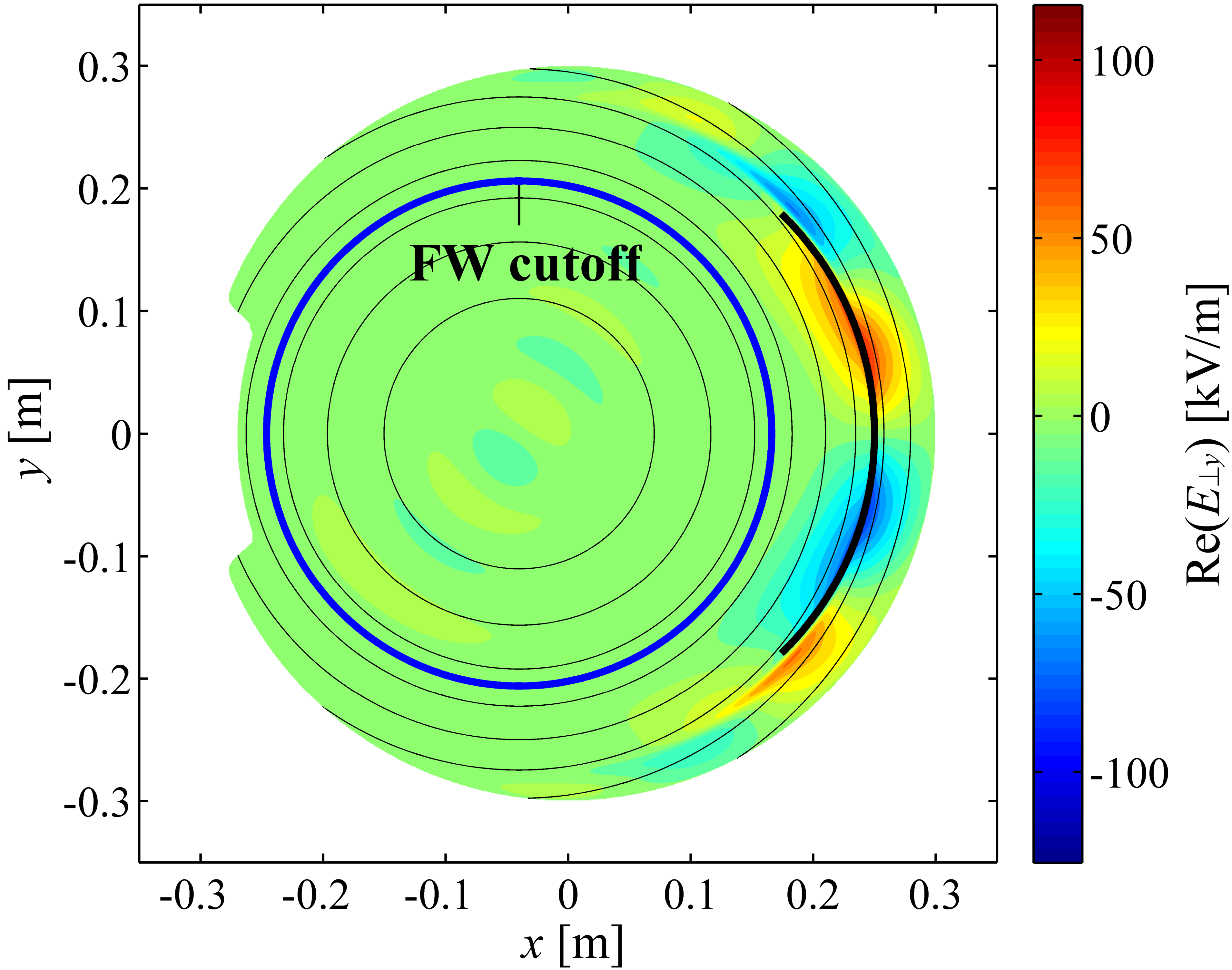

FW cutoff
0.3
0.2
0.1
0
-0.1
-0.2
-0.3
y [m]
x [m]
100
50
0
-50
-100
Re($E_{\perp y}$) [kV/m]

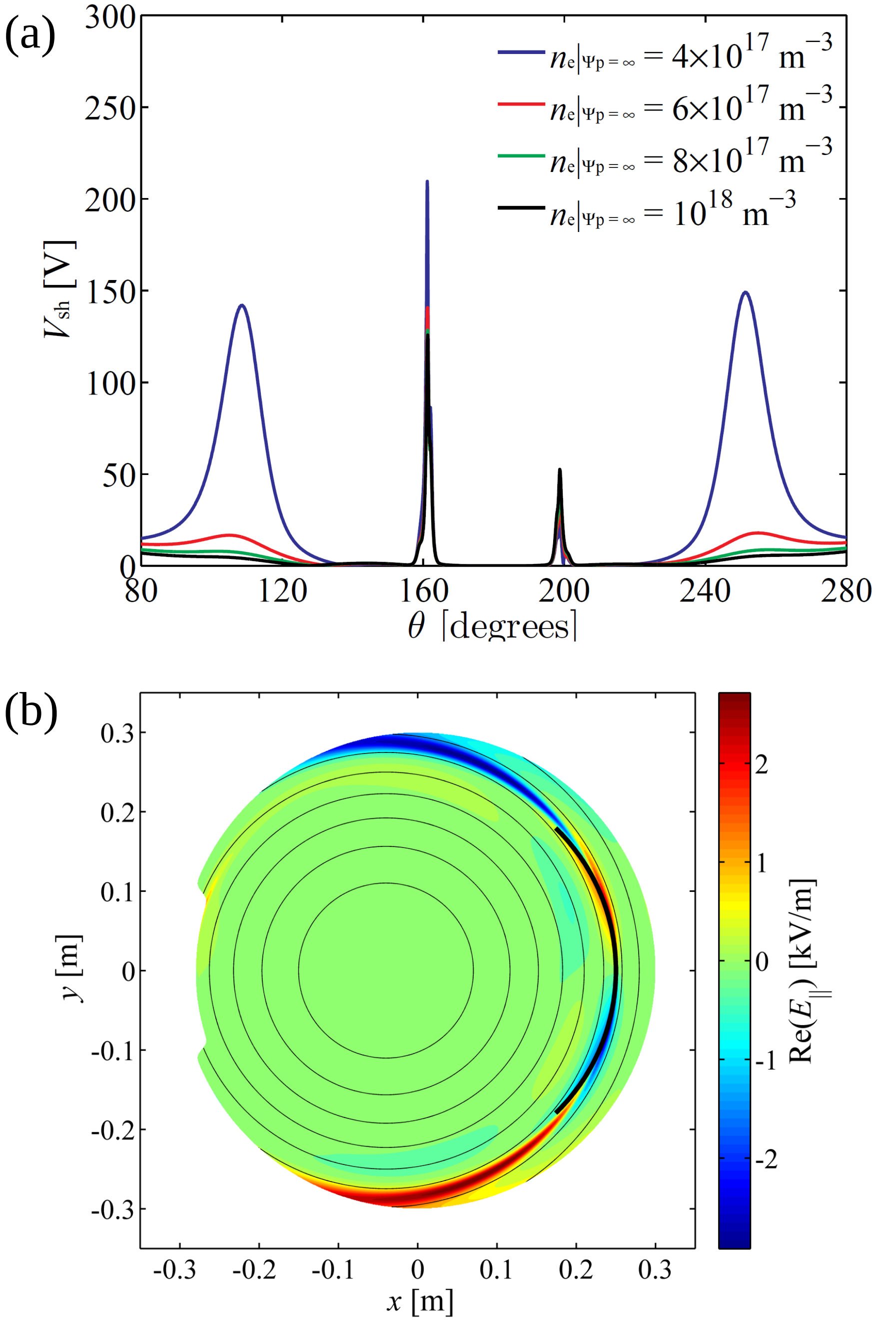

(a)
$n_e|_{\Psi_p=\infty} = 4\times10^{17}$ m^{-3}
$n_e|_{\Psi_p=\infty} = 6\times10^{17}$ m^{-3}
$n_e|_{\Psi_p=\infty} = 8\times10^{17}$ m^{-3}
$n_e|_{\Psi_p=\infty} = 10^{18}$ m^{-3}
V_{sh} [V]
θ [degrees]
(b)
y [m]
x [m]
Re($E_{||}$) [kV/m]

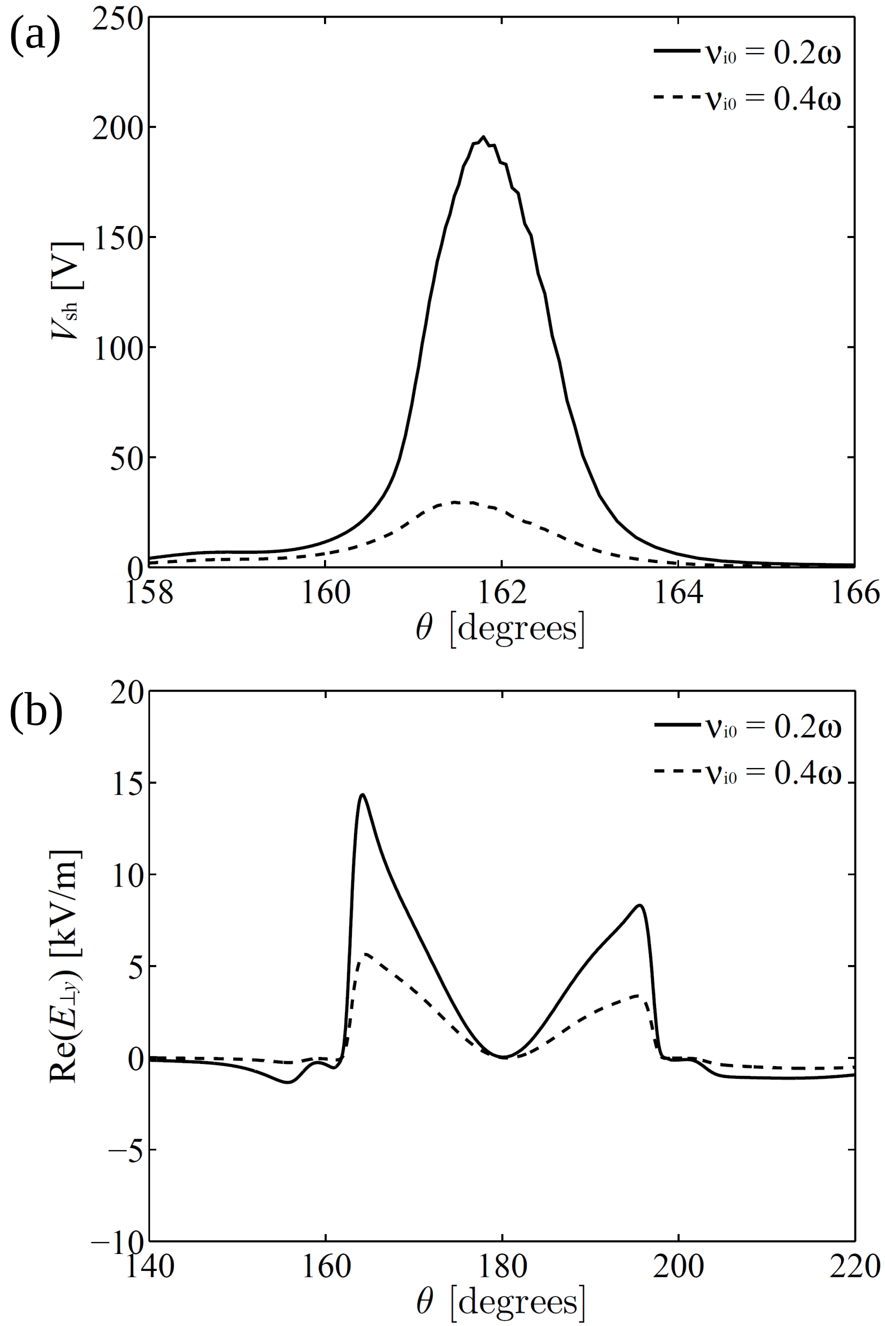

(a)
V_{sh} [V]
θ [degrees]
$\nu_{i0} = 0.2\omega$
$\nu_{i0} = 0.4\omega$
(b)
Re($E_{\perp y}$) [kV/m]
θ [degrees]
$\nu_{i0} = 0.2\omega$
$\nu_{i0} = 0.4\omega$